Available online at www.eccomasproceedia.org
Eccomas Proceedia COMPDYN (2023) 798-815

ECCOMAS
Proceedia

COMPDYN 2023
9th ECCOMAS Thematic Conference on
Computational Methods in Structural Dynamics and Earthquake Engineering
M. Papadrakakis, M. Fragiadakis (eds.)
Athens, Greece, 12-14 June 2023

EQUIVALENCE OF DAMPING PROPERTIES OF DISSIPATIVE DEVICES FOR MITIGATING THE SEISMIC RISK OF RIGID BLOCKS

Linda Giresini[1,*], Omar AlShawa[1], Luca Umberto Argiento[2], and Claudia Casapulla[3]

[1] Department of Structural and Geotechnical Engineering, University of Rome La Sapienza
Via Eudossiana 18, 00184 Rome (Italy)
*Corresponding author, e-mail: {linda.giresini,omar.alshawa}@uniroma1.it

[2] Department of Engineering, University of Napoli 'Parthenope'
Centro Direzionale is.C4, 80143 Neaples (Italy)
e-mail: archargiento@libero.it

[3] Department of Structures for Engineering and Architecture, University of Napoli Federico II
Via Forno Vecchio 36, 80134 Naples (Italy)
e-mail: casacla@unina.it

Abstract

Non-structural elements, such as infill walls, precast r.c., timber panels, machines, cabinets, art objects, etc. can be considered as rigid rocking blocks whose seismic vulnerability may be reduced by means of dissipative and recentering devices. These devices can be installed in different positions of the rigid block. This paper proposes an equivalence criterion to compare dashpots installed either at the base or at the top of rocking blocks in terms of damping coefficients. An analytical expression is obtained and validated through deterministic and stochastic approaches. The first aims to compare the two scenarios' performances, while the second introduces a probabilistic assessment in terms of fragility curves and seismic demand hazard. The comparisons exhibit an optimal agreement, making the analytical formulation reliable for design purposes.

Keywords: rocking; seismic isolation; damping, equivalent viscous coefficient; energy dissipation

ISSN:2623-3347
Peer-review under responsibility of the organizing committee of COMPDYN 2023.
doi: 10.7712/120123.10436.20470

1 INTRODUCTION

The seismic protection of non-structural components such as infill walls, precast r.c., timber panels, machines, cabinets, and art objects is a known issue to deal with, especially for the high direct and indirect costs caused by their damage. For example, one of the main non-structural components potentially dangerous for frame structures are infill panels/partitions, since their role is generally neglected or not sufficiently investigated in the overall seismic response of buildings [1]. For them, a low-damage solution may consist in an articulated mechanism or jointed system capable of accommodating inter-story drifts through internal rocking mechanisms with inelastic behavior concentrated where dissipative/recentering devices are placed (Figure 1).

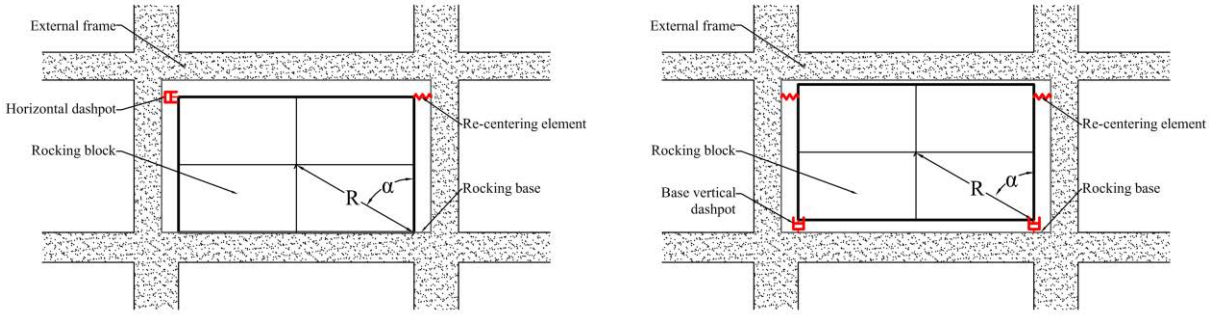

(a) (b)

Figure 1: Rocking isolation with viscous dampers installed at a certain height (a) and at the base of the panel (b).

Other rigid blocks are machines in hospitals or in plants, artistic assets, museum objects that can rock during earthquakes. Dissipative devices can then be installed to reduce their seismic vulnerability, coupling them to self-centering components or tendons. Such a coupling constitutes a hybrid system associated to a flag-shape force-displacement relationship very good from a seismic point of view, as implies energy dissipation and at the same time zero residual displacement during the cyclic response. The viscous-elastic damper can be located at the base of the rocking block [2] or to a certain height from its base with the purpose of mitigating the seismic vulnerability. The perspective is the same as that adopted in the damage avoidance design, which protects the structure from damage allowing motion [3], [4] Analytical and numerical approaches have been provided studying the uplifting of anchored blocks [5], [6], and similar approaches have been applied to masonry structures to study the behavior of masonry walls restrained by tie-rods [7]–[9]. Some other contributions, including their seismic assessment through probabilistic approaches, were related to furniture, electric or mechanical equipment anchored at the base [10]–[13]. This work proposes an equivalence criterion between damping properties of these different passive control systems with respect to their position. Such an equivalence may ease the design of dissipative and re-centering components in the case of installation constraints.

More in detail, Section 2 contains the analytical background and the equivalence criterion proposed for calculating the damping properties of dissipative devices located either at the base or at the top of rocking rigid walls. Section 3 validates this equivalence through a deterministic analysis of two rigid blocks with different slenderness, rocking in-plane and out-of-plane. Moreover, it discusses the effects of dissipative and re-centering components on the rocking response. Sections 4 and 5 discuss the stochastic analyses performed to validate the equivalence criterion and to define the seismic demand hazard curves for the panels freely rocking and rocking-isolated.

2 EQUIVALENCE CRITERION

2.1 Hypotheses

The equivalence criterion is presented referring to the classical Housner's formulation [14], [15] for which the seismic excitation is horizontal; the rigid block rocks over an infinitely stiff foundation without either sliding or bouncing. The horizontal elastic restraint is active only up to its own yielding value, after which its contribution vanishes.

2.2 Equivalence criterion

The equations of motion of a block purely rocking around its base corners can be obtained through the Euler-Lagrange's formulation. The block can be either free-standing or connected to a fixed support via vertical or horizontal dissipative restraints, in which elastic and/or viscous forces may develop. These represent the connections of the rigid panel to the structural elements.

The block is geometrically defined by its size R and its slenderness ratio α, arctangent of thickness to height ratio (Figure 1).

When a rectangular block of mass m and inertia moment I_0 (Figure 1b) is connected to a damper of equivalent viscous coefficient c_{top} installed at a certain height from the base, the equation of motion reads:

$$I_0\ddot{\vartheta} + sgn(\vartheta)mgR\sin A_\vartheta + \\ +sgn(\vartheta)\,K\beta^2R^2\cos A_{r,\vartheta}\,\left[\sin\alpha_r - \sin A_{r,\vartheta}\right] + c_{top}\,\beta^2R^2\,cos^2\,A_{d,\vartheta}\,\dot{\vartheta} = m\,\ddot{u}_g R\,cos\,A_\vartheta \quad (1)$$

where $\vartheta = \vartheta(t)$ is the rotation dependent on time that is defined through the solution of the equation of motion. Generally, the displacement time-history is expressed in normalized terms as ϑ/α. By using statistical analysis, the corresponding engineering demand parameter (EDP) for each realization is the maximum ϑ_{max}/α registered over the individual earthquake time. This EDP is normally selected [16], [17] when the motion is pure rocking since the block returns, if stable, to its original position virtually without any permanent deformation or damage. K in Eq. (1) is the stiffness of a horizontal restraint whose position is defined by $R_d = \beta R$, being β a scalar coefficient variable from 0 (no restraint) to 2 (restraint at the top corner). The term depending on K is calculated as explained in [18]. Similarly, through the Euler-Lagrange's formulation, the term depending on c_{top} is obtained (see [19] for further details). The arguments of the sinusoidal functions are:

$$A_\theta = \alpha - sgn(\vartheta)\cdot\vartheta;\; A_{r,\vartheta} = \alpha_r - sgn(\vartheta)\cdot\vartheta;\; A_{d,\vartheta} = \alpha_d - sgn(\vartheta)\cdot\vartheta \quad (2)$$

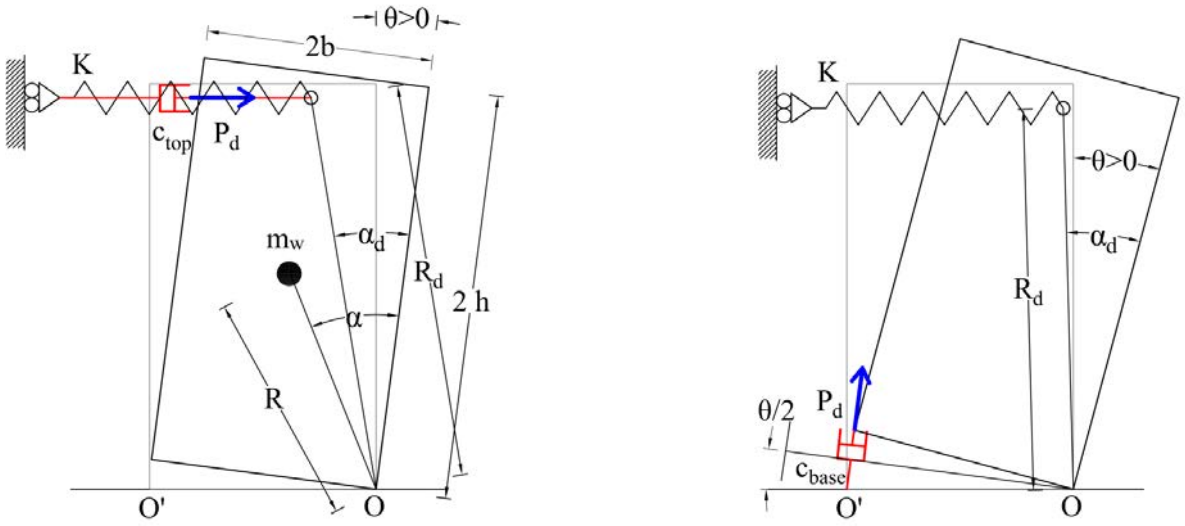

(a) (b)

Figure 1: Schematics of the rocking block restrained by horizontal (a) and base vertical damper (b) recentered by a horizontal re-centering component.

If the damper is at the base of the rigid block (Figure 1b), with c_{base} as the equivalent viscous coefficient, Eq. (1) becomes:

$$I_0\ddot{\vartheta} + sgn(\vartheta)mgR\sin A_\vartheta + \\ +sgn(\vartheta)\,K\beta^2R^2\cos A_{r,\vartheta}\,\left[\sin\alpha_r - \sin A_{r,\vartheta}\right] + 2\,c_{base}\,R^2\,sin^2\,\alpha\,\,(1+\cos\vartheta)\,\dot{\vartheta} \\ = m\,\ddot{u}_g R\,cos\,A_\vartheta \tag{3}$$

The term of Eq. (3) depending on damping was found by Dimitrakopoulos and DeJong in [2]. The damping force is here assumed linearly variable with the velocity. It is intended that the vertical dashpot shown in Figure 1b is also present in O when rocking is counterclockwise; so two dashpots are assumed as depicted in **Errore. L'origine riferimento non è stata trovata.**b.

The equations for the free-standing configurations are simply obtained from Eqs. (1) and (3) with the condition $K = c_{top} = c_{base} = 0$. The transition from the equations valid for restrained blocks to those suitable for free-standing blocks is considered with a fracture function proposed by (Makris and Black 2002) [5], [6] so expressed:

$$f(\vartheta) = 1 \text{ when } \vartheta(t) > \vartheta_y \\ f(\vartheta) = 0 \text{ when } \vartheta(t) \le \vartheta_y \tag{4}$$

where ϑ_y is the block rotation corresponding to the yielding of the horizontal restraint.

2.3 Remarks on the energy dissipation and on the equivalent damping

As already pointed out, in the rocking behavior of free-standing blocks, there is only one source of energy dissipation, given by the impact of the block itself on the ground, assumed as infinitely rigid. Housner theorized it as a coefficient of restitution (COR) given by the ratio of kinetic energy just after an impact to that just before the impact [20]. Later, Aslam et al. [21] expressed it as a ratio of the two corresponding velocities. In the simplest form of rocking be-

havior, both bouncing and sliding are disregarded: this hypothesis is always valid for enough slender blocks with h/b greater than 4 [22]. In more recent years, researchers were also focused on the effect of horizontal and vertical restraints added to rocking blocks [5], [18], [23]–[26]. When the block is connected to a viscous damper or to a generic restraint, either at its base or at a certain height, there is an additional source of energy dissipation. Indeed, as shown by experimental tests, additional restraints could cause a reduction of the COR, namely an increase of energy loss in the case of restrained rocking blocks [14], [27]. Such a reduction influences the experimental value of the COR, which is even lower than the analytical one found by Housner [14], [15]. Indeed, the experimental COR for masonry rocking blocks results to be about 90-95% of the analytical value, since it may also take into account some local plastic deformations [28]For rectangular blocks, the analytical value is equal to 1-1.5 (sin2α), where $\alpha = b/h$ measures the slenderness ratio of the block as the ratio of thickness to height (Figure 1). If the block is stocky, the slenderness ratio is the arctangent of the ratio of thickness to height.

The criterion to compare the damping properties of dissipative devices in both positions (top and base) equates the two terms of Eqs. (1)-(3) in the case of free vibrations (with $K = 0$ and $\ddot{u}_g = 0$). Considering the exponential solutions of the homogeneous differential equations (similar to that reported in [29] for the SDOF equivalent oscillator), it is straightforward to observe that the solution is the same once the terms depending on the damping coefficient are equal.

Bearing in mind that c_{base} is the equivalent viscous coefficient of the base (vertical) dissipator, whereas c_{top} is that of the top (horizontal) dissipator (Figure 1), the equivalence between the effects of the two dissipative devices will provide:

$$c_{base}\ 2R^2\ sin^2\ \alpha\ \ (1+\cos\vartheta)\dot{\vartheta} = c_{top}\ \beta_d^2 R^2\ cos^2\ A_{d,\vartheta}\ \ \dot{\vartheta} \tag{5}$$

from which, if the rotation angles are small:

$$\frac{c_{base}}{c_{top}} = \frac{\beta_d^2\ cos^2\ A_{d,\vartheta}}{2\ sin^2\ \alpha\ \ (1+\cos\vartheta)} \cong \frac{\beta_d^2}{4}\frac{cos^2\ \alpha_d}{sin^2\ \alpha} \tag{6}$$

valid if $\vartheta \ll \alpha$. The relationship between the dimensionless ratio c_{base}/c_{top} and α is reported in Figure 2a. Assumed that the dashpot is located in symmetric position as in Figure 1a, the relationship between α and α_d is:

$$\alpha_d = \text{arcsen}\left(\frac{sen\ \alpha}{\beta_d}\right) \tag{7}$$

If the damper is located at the top of the rocking block ($\beta_d = 2$) and if $\alpha_d \cong \alpha$, the ratio between the coefficients of base damper to top damper is:

$$\frac{c_{base}}{c_{top}} \cong \frac{1}{tan^2\ \alpha} \tag{8}$$

The latter approximated expression is compared to the exact expression (Eq. (6) for small rotations) in Figure2b; one can observe that they basically coincide for $0.0 < \alpha \leq 0.5$.

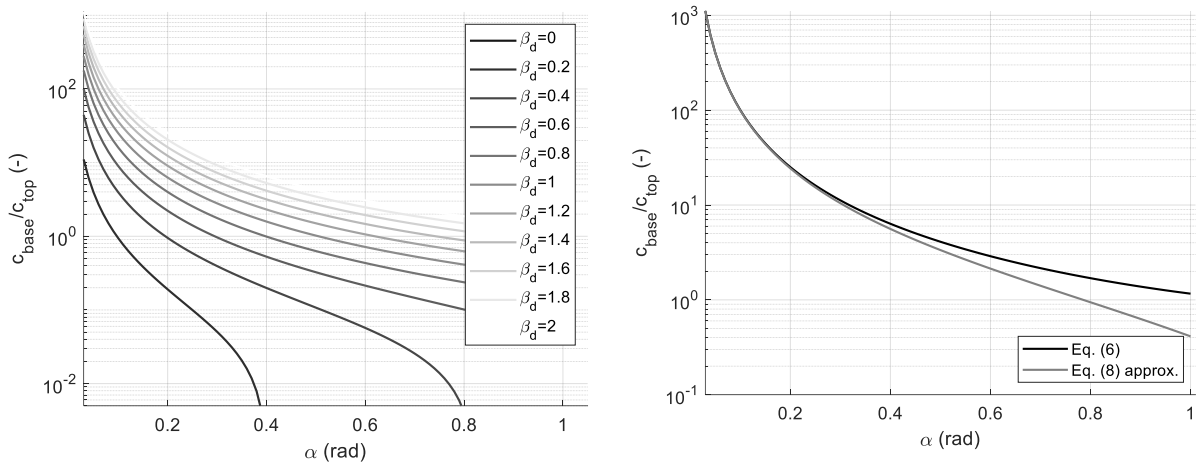

(a) (b)

Figure 2. Ratio of damping terms base dissipator/ top dissipator with variable $\boldsymbol{\beta_d}$ as in Eq. (6) (a); damper at the top of the wall ($\boldsymbol{\beta_d = 2}$), comparison between approximated (Eq. (8)) and exact (Eq. (6)) expressions (b).

Looking at Figure 2b, the following considerations can be made:

- The c value to assume if the dissipator is at the base is remarkably greater than that to assume if the dissipator is at a certain height from the ground for slender blocks. This is expected, as the effective lever arm of the base dissipator is very low for slender blocks;
- For $0.1 \leq \alpha < 0.8$, corresponding to wall slenderness values commonly found in civil engineering, the c value of the base dissipator should be greater than that at the top, in order to be equivalent;
- For $\alpha > 0.8$, that is for stocky blocks, this trend is reversed if the approximated expression is used; in fact, the base dissipator gives a lower effect than that horizontal at the top. If the correct expression (Eq. (6) is assumed, the damping of the base dissipator is always greater than that at the top;
- For $\alpha = 1.0$ the dissipator, independently from its position, has the same "pseudo-static" effect.

The equivalence criteria reported in Eqs. (6)-(8) are trivially valid for a free-vibration problem, but their validity is not predictable when dealing with forced vibrations, especially since the input excitations are earthquakes with complex frequency contents. Therefore, the following sections aim at validating the equivalence criterion proposed to ease the design of dissipative and re-centering components often subjected to installation constraints.

3 DETERMINISTIC ANALYSIS

3.1 Selection of parameters and records

Two rigid blocks are considered: a slender wall rocking out-of-plane (OOP) and a stockier wall rocking in-plane (IP). The first typology may represent masonry or r.c. walls connected to frame structures through earthquake resistant devices conceived considering damage avoidance design, whilst the second may regard panels of whatever material rocking in-plane

with similar connections (Figure 1). Two rectangular block geometries are considered: the first type is a block of dimensions (height x width x thickness) 2.70x1.52x0.25 m^3, while the second is 2.70x0.40x2.70 m^3 (see Figure 3). Both specimens are assumed to have a specific weight of 19 kN/m3; the consequent mass and geometric properties are reported in Table 1. The first wall rotates around the axis along its width, whereas the second one rocks around the axis along its thickness. For both typologies, the free condition ($c = K = 0$) is firstly analyzed, and then dampers and re-centering devices (equivalent springs) of variable damping coefficient c and stiffness K are considered, respectively, as vertical and horizontal restraints. Bouncing and sliding are neglected in both cases. Non-linear dynamic analyses are performed under two seismic records of medium-high intensity with similar peak ground acceleration (PGA) and peak ground velocity (PGV), intensity measures usually considered for rocking analysis. For the stocky block, an amplification of the acceleration time- history by 8.8 has been considered to trigger motion in it. Indeed, the minimum acceleration needed to make the block rotate is $\tan\alpha$.

Block type	Mass [kg]	Slenderness ratio $\boldsymbol{\alpha}$ [-]	Radius vector R [m]	c [N/m/s]	$\frac{c_{base}}{c_{top}} = \frac{1}{tan^2\,\alpha}$ *
Slender (OOP)	1960	0.09	1.40	0-1000	123
Stocky (IP)	5540	0.79	1.78	0-1000	1

Table 1: Geometric parameters of the analyzed blocks (OOP=out of plane, IP=in plane) *from Eq. (8).

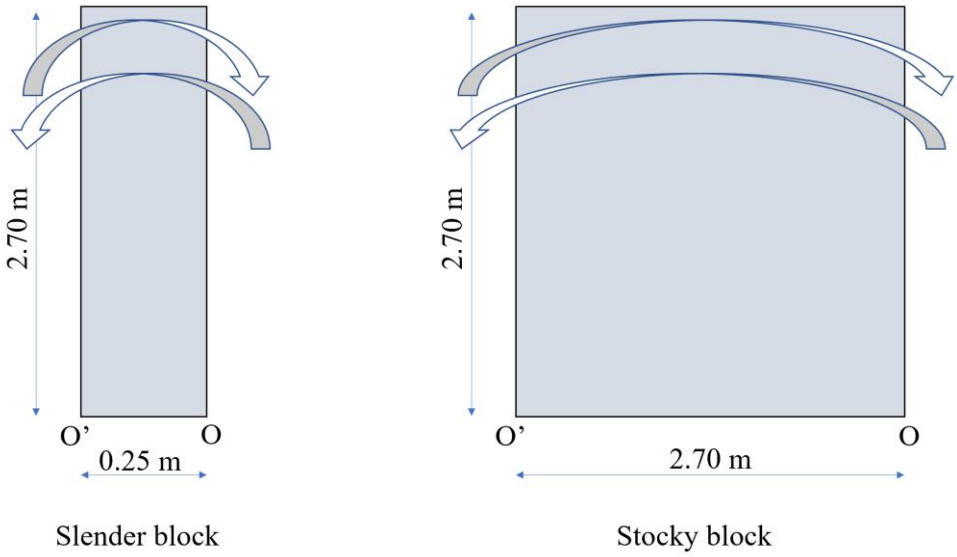

Figure 3: Geometries of the analyzed blocks.

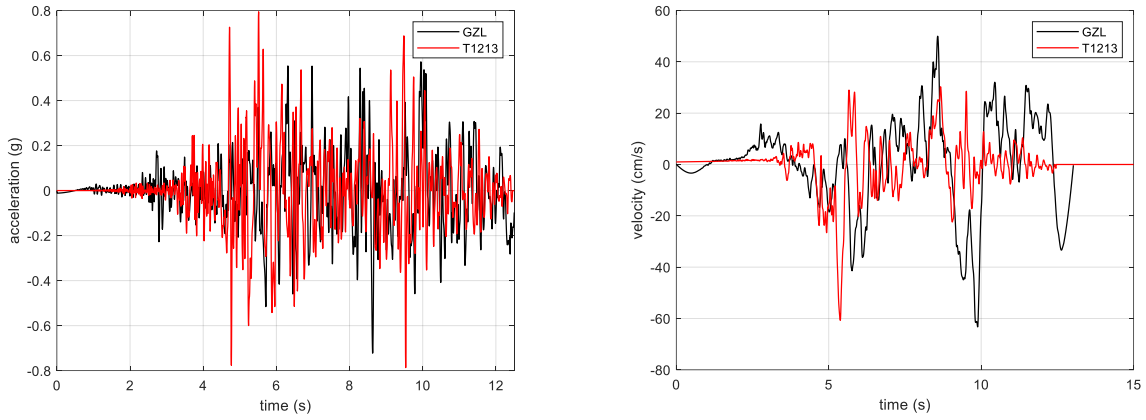

(a) (b)

Figure 4: Acceleration (a) and velocity (b) time-histories used for the deterministic analyses.

The minimum amplification factor for the stocky block would be then PGA/$\tan\alpha$; nevertheless, this value generates almost negligible rotations. To make a direct comparison between the two blocks, the same ratio between PGA/$\tan\alpha$ is hence considered: therefore, for the stocky block the amplification factor is the ratio between the two values of $\tan\alpha$: 0.79/0.09= 8.8. As for the COR, the value assumed for the slender block is 0.8 times that proposed by Housner, considering the reduction observed to occur in experimental tests [14]. Nevertheless, for the stocky block, the analytical value proposed by Housner is not considered to avoid too small rotations. Thus, the same COR adopted for the slender block has been assumed (e =0.79). Moreover, the same COR guarantees the same energy dissipation due to impacts between the two configurations, so to make the comparison between them characterized by the same parameter. A specifically written MATLAB code uses the 4th-5th order Runge-Kutta integration technique to solve the equations of motion (Eqs. (1)-(3)) for rocking blocks restrained in different configurations. Then, comparisons are made to understand the role of the damper position in the dynamic responses of the two rocking panels under two emblematic ground motions (Figure 4) via a deterministic approach. The corresponding IMs are respectively for GZL and T1213 earthquakes: PGA=708 cm/s^2 and PGA=779.3 cm/s^2 (Figure 4a); PGV=63.3 cm/s and PGV=60.7 cm/s (Figure 4b).

3.2 Discussion of results

As for the slender block, rocking OOP, the normalized rotation ϑ/α time-histories are reported for the free wall (c =0) and for the cases with base and top dissipator, both with and without the re-centering component, whose parameter is K. In the figures, the legend indicates the value of the damping coefficient, the stiffness of the re-centering spring and the position of the dissipator (base or top). Although the acceleration and velocity based intensity measures of the two earthquakes are similar (Figure 4), the free wall overturns under GZL (which has a slightly greater PGV than T1213) and is stable under T1213 (Figure 5). That demonstrates the strong influence of the seismic input on the response: even small variations of it may cause a very different response. Moreover, this aspect confirms that the PGV is a more significant parameter to cause overturning.

As expected, the addition of a base or of a top damper makes the block stable with maximum normalized rotations less than 1.0, with the exception of the base-isolated wall without recentering component, K=0 (Figure 5b). In this case, the dissipative force of the damper is

not capable of recovering the destabilizing action of the inertia force of the block due to the seismic input. The black curves in Figure 5 refer to a stiffness value of the re-centering component equal to zero, whereas the red curves refer to a flat value of K=1E4 N/m (for the sake of comparison, a steel tie-rod with diameter 12 mm and length 5 m corresponds to K=4.8E5 N/m). It is evident that a re-centering component, even with low stiffness if compared to that just mentioned), furtherly mitigates the motion amplitude, making it smoother.

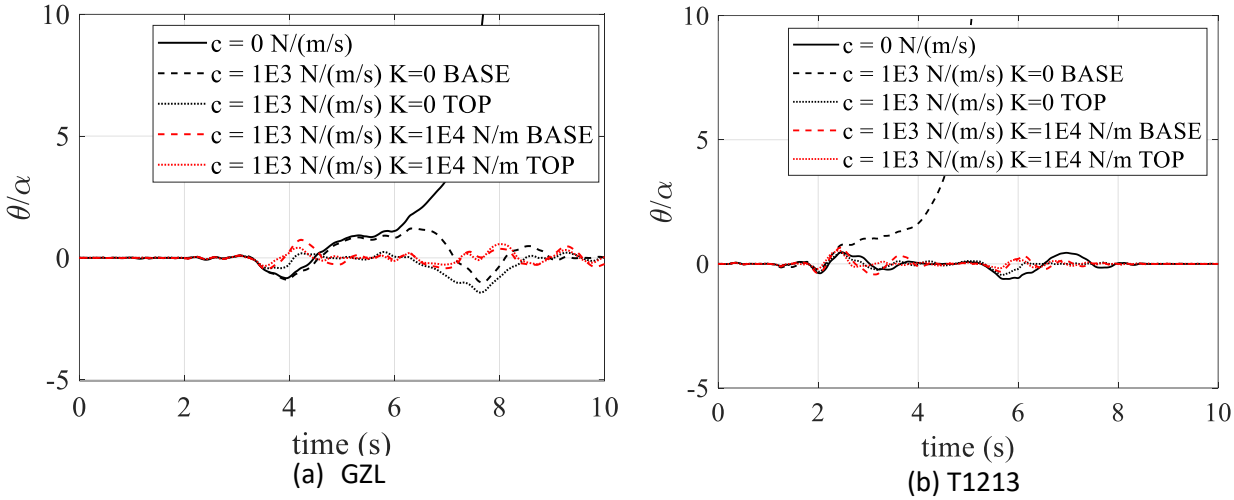

Figure 5: Slender block OOP, variable $\boldsymbol{c}$ and $\boldsymbol{K}$: GZL earthquake (a); T1213 earthquake (b).

Limiting the observations to the dampened conditions, both with and without re-centering component, from Figure 6 it is clear that there is a correlation between damping properties of the base dissipator and those of the top dissipator. Indeed, if one assumes the same damping coefficient for the two positions for the base dissipator and the top dissipator, the response is quite different (black curves in Figure 6a and Figure 6b). Taking into account the equivalence expressed by Eq. (8), it results that the equivalent damping coefficient of the base dissipator should be assumed as the coefficient of the dissipator at the top of the block multiplied by a factor $\frac{1}{tan^2 \alpha} = 123$ (α =0.09). Doing so, the response time-history is very similar for the cases of top and base dissipator, as visible comparing the continuous black curves (top dissipator) and the dashed red lines (base dissipator with properly increased damping) in Figure 6. Therefore, the equivalence expressed by Eq. (8), or, in the more general case, Eq. (6), can be considered as a design indication to pass from top dampers to base dampers or vice-versa. Only slight differences, noted in the second part of the response – and therefore perhaps due to accumulation of numerical errors – are observed in Figure 6b and Figure 6c, but all the comparisons show a more than satisfactory agreement. Then, although the rocking problem is intrinsically non-linear, the equivalence derived from analytical considerations can be so far considered acceptable.

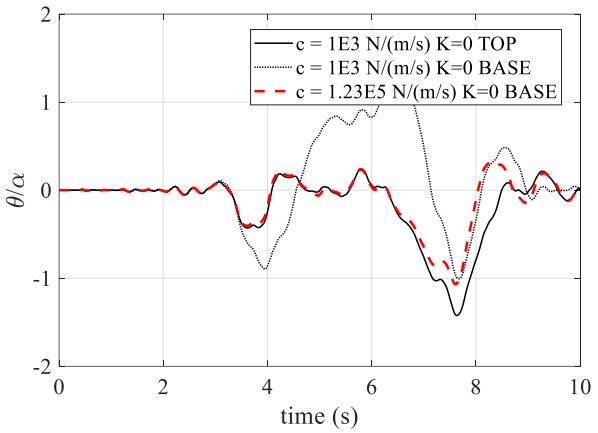

GZL
(a)

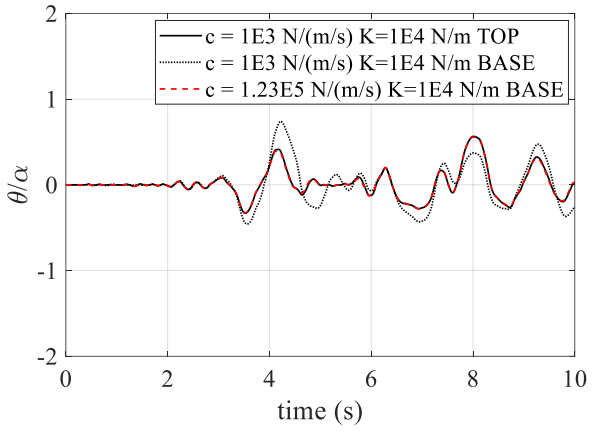

GZL
(b)

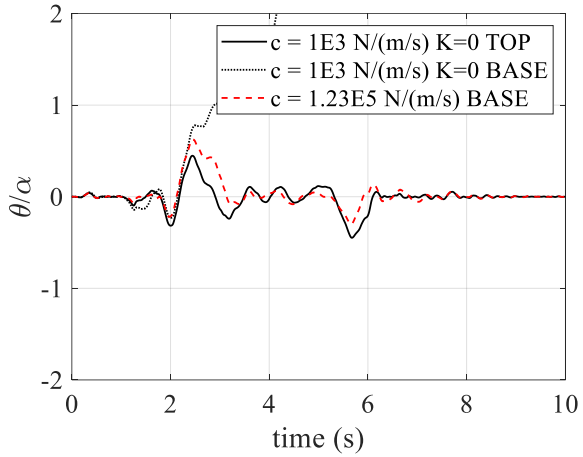

T1213
(c)

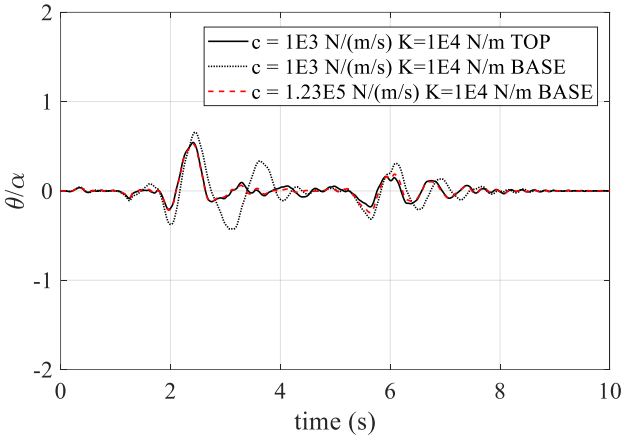

T1213
(d)

Figure 6: Slender block OOP, GZL: $\boldsymbol{K}$=0 (a) or $\boldsymbol{K}$=1E4 N/m (b); T1213: $\boldsymbol{K}$=0 (c) or $\boldsymbol{K}$=1E4 N/m (d) and variable $\boldsymbol{c}$

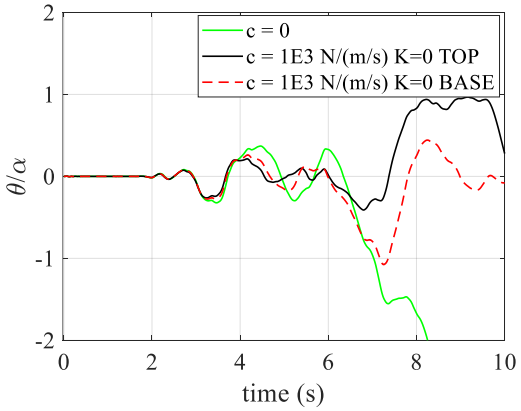

GZL
(a)

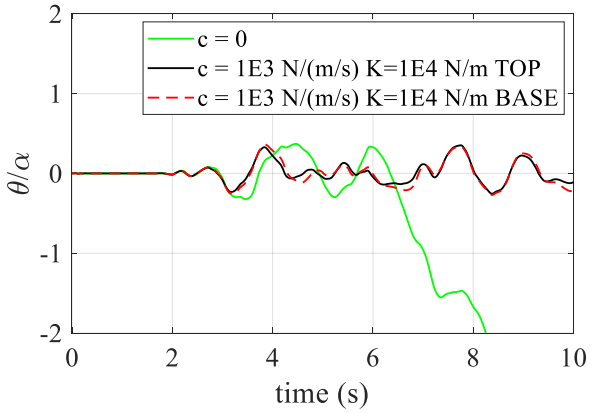

GZL
(b)

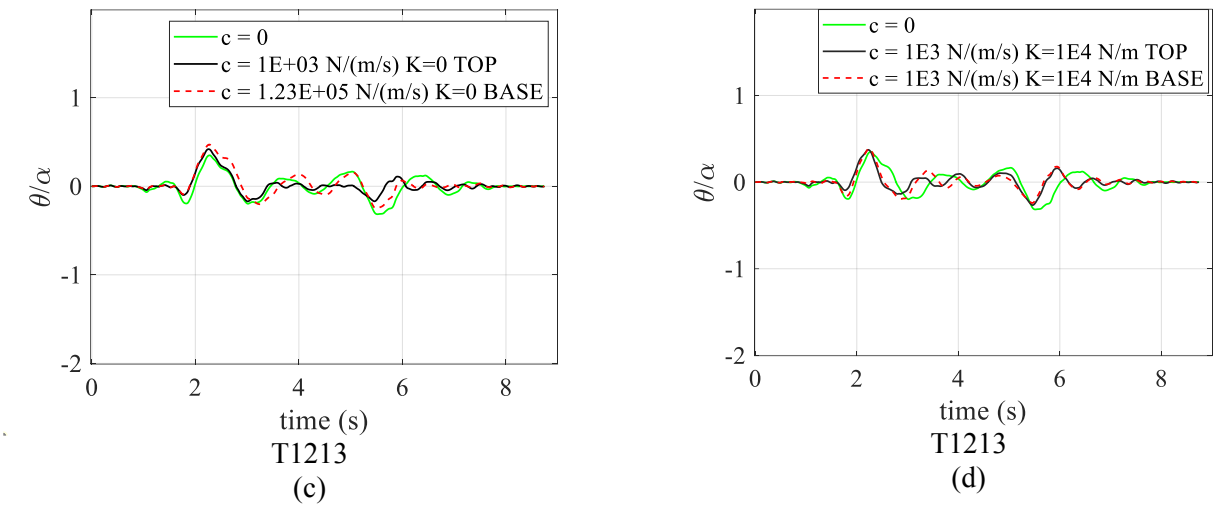

Figure 7: Stocky block IP, GZL: $\boldsymbol{K}$=0 (a) or $\boldsymbol{K}$=1E4 N/m (b); T1213: $\boldsymbol{K}$=0 (c) or $\boldsymbol{K}$=1E4 N/m (d) and variable $\boldsymbol{c}$.

Analogous results are obtained for the stocky block rocking in-plane. Indeed, as visible in Figure 7, the base dissipator with the equivalent viscous coefficient ($\frac{c_{base}}{c_{top}} = \frac{1}{tan^2\,\alpha} = 1$ as reported in Table 1) provides very similar rotation time-histories as the wall restrained by the top dissipator. Again, the best agreement is observed for the situation with the re-centering component (Figure 7b,d), whereas in absence of it the agreement is good for the first part of the response time-history (Figure 7a,c). These curves are calculated with the COR equal to that assumed for the slender block (e=0.79). A COR closer to the Housner's analytical value (e=0.25), causes (results not reported here) a remarkably lower number of impacts, resolving the problem of response difference in the second part of the time-history. Finally, it is worth noting that the rocking analyses of stocky block should account for bouncing and sliding, which in this case have been neglected for the sake of simplicity.

4 STOCHASTIC VULNERABILITY ANALYSIS

4.1 Methodology

The equivalence between different properties of dampers is now investigated through a stochastic analysis. As illustrated in the following, fragility curves are calculated and compared for different configurations of the rocking block connected to base damper and top damper to test the equivalence proposed in Section 2. The limit states are the same as those considered in [17], [30]. In summary, the thresholds considered for the limit states are:

1. LS0, rocking initiation, $EDP > 0.0$;
2. LS1, limited rocking, $EDP = 0.1$;
3. LS2, moderate rocking, $EDP = 0.4$;
4. LS3, near-collapse rocking, $EDP = 1.5$.

The limit states LS_1 and LS_2 can be seen as serviceability limit states, whereas LS_3 as an ultimate limit state.

The fragility curves are obtained with the same procedure explained in detail in [17], [30].

4.2 Selection of parameters for the probabilistic analysis

4.2.1 Intensity measures

Classical ground motion parameters related to rocking walls are PGV, PGA, PGD (peak ground displacement), the ratio of PGV and PGA, the Housner's spectrum intensity SI_H. Acceleration-based parameters are the Arias intensity I_a and the root-mean-square acceleration RMSA, which are more representative for short period structures [31], and the cumulative absolute velocity CAV [32]. Additional IMs used are the strong motion duration t_D [33], the mean period T_m [34] and the characteristic length scale [31]. All the expressions of the mentioned IMs and used in the following subsections are thoroughly described in [35].

4.2.2 Selection of seismic records

The list of 20 seismic records used in the probabilistic analyses is reported in Table 2. These earthquakes have been taken from the Engineering Strong-Motion database (ESM [36]) considering the 2016 Central Italy Earthquake swarm (label of earthquakes beginning with "2016"). Moreover, other seismic records registered worldwide have been selected choosing a magnitude greater than 4.0 and PGV values greater than 30 cm/s. The choice of PGV as a parameter depends upon the strong influence that PGV has on the rocking response of rigid blocks [37], as also demonstrated in Section 3. The selected seismic inputs should be filtered considering the dynamic behavior of the building IP and OOP rocking infill panels at a certain height of the foundation. In the latter case, however, the filtering effect cannot be standardized with trivial scaling factors, especially when dealing with non-linear transient analysis. To simplify, here the seismic inputs have been assumed without filtering them, in other words considering the behavior of the main structure as rigid.

Record date_ station	PGA [cm/s^2]	PGV [cm/s]	PGV/PGA [s]	PGD [cm]	SIH [cm]	I_a [cm /s]	I_v [cm^2/s]	t_D [s]	IF [cm$^{5/4}$/s]	RMSA [cm/s^2]	RMSV [cm/s]	RMSD [cm]
19760517_GZL	709	63	0.09	21	206	481	3970	24	141	150	17	7
19760915_GMN	632	68	0.11	12	231	240	2707	12	128	116	16	3
19770304_A39	166	31	0.19	10	133	40	1346	2	37	33	7	3
19780916_TAB	823	86	0.10	33	311	1031	10664	52	231	169	21	12
19801123_STR	310	70	0.23	27	170	137	4730	7	114	69	17	9
19900620_A6211	573	37	0.06	10	131	413	1471	21	79	116	9	3
19920313_2402	478	77	0.16	28	210	172	4082	9	132	101	19	10
19940620_A3297	995	32	0.03	4	58	592	353	30	75	131	4	1
19950615_AIGA	489	40	0.08	8	118	98	634	5	59	60	6	1
19991112_1401	808	66	0.08	11	241	241	3165	12	123	80	11	2
19991112_8101	515	83	0.16	56	269	295	13571	15	162	117	32	23
20160824_2_FOC	175	3	0.02	0	6	19	4	1	3	38	1	0
20160824_NRC	353	29	0.08	10	106	102	577	5	43	91	8	5
20161026_2_CMI	707	56	0.08	6	130	242	910	12	104	112	9	1
20161026_CLF	122	12	0.10	2	44	21	188	1	12	29	3	1

20161026_CMI	638	43	0.07	14	140	225	921	11	79	154	11	6
20161026_FOC	612	20	0.03	2	31	201	159	10	36	102	4	1
20161026_MNF	119	8	0.07	5	23	8	35	0	7	24	2	3
20161030_ACC	426	44	0.10	13	138	199	1106	10	78	123	12	4
20161030_NOR	303	50	0.17	23	208	162	2765	8	85	61	10	6

Table 2: List of seismic records used in the probabilistic analyses: PG-A-V-D Peak Ground Acceleration, Velocity, Displacement; SIH Spectrum or Housner Intensity; I_a Arias Intensity; I_v Energy Density; t_d strong motion duration; IF Fajfar Index; RMS-A-V-D Root Mean Square Acceleration, Velocity, Displacement.

4.3 Fragility curves

The univariate fragility curves are calculated to assess the equivalence between the effects of different dampers located at the base and at the top of the two considered rocking blocks. As for the slender block, the results for the undamped and the damped block with horizontal dissipator at the top are displayed in Figure 8. The optimal IM are selected to represent the fragility curves according to the procedure described in [35], that are in this case PGV and I_V. For all the limit states (Figure 8a), the addition of a dissipator strongly reduces the seismic vulnerability of the wall. Nevertheless, this improvement is not particularly visible for the case of limited rocking LS_1 (black solid and dot curves in the figure). The beneficial effect of mitigation of motion is instead much more visible for moderate and near-collapse rocking. For these reasons, the comparison between the cases when the dissipator is located in different positions is more effective for LS_2, in order to test the accuracy of the equivalence even when the differences with the undamped case are minimal but the rotations are quite high. Observing Figure 8b and Figure 9 (stocky block rocking IP), it is evident that a very good agreement in terms of conditional probability is obtained for the case of base and top dissipators having damping coefficient calculated with the proposed equivalence criterion.

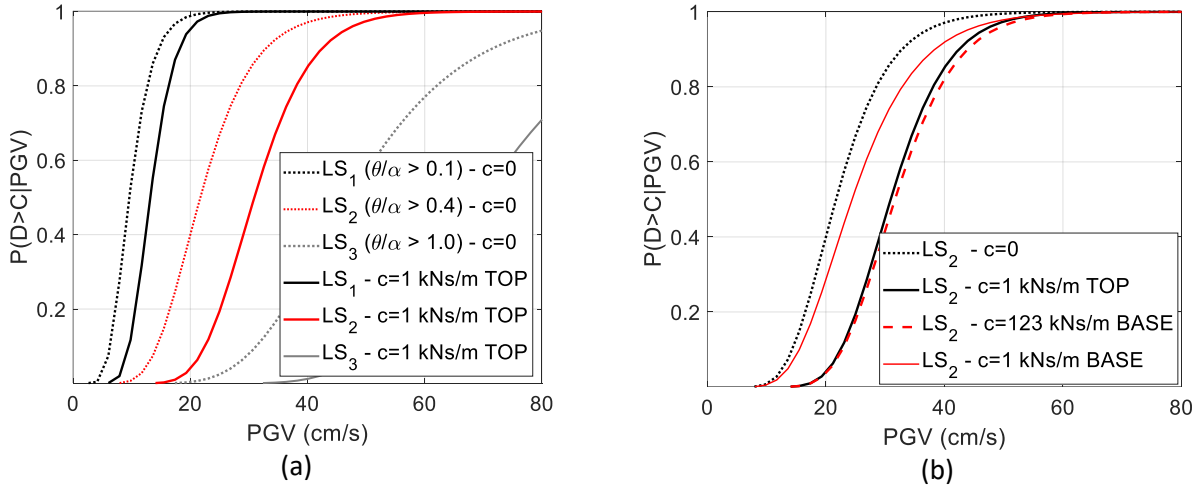

Figure 8: Fragility curves for slender block OOP: variation of probability of failure for all the limit states (a); comparison of damped configurations with undamped configuration for moderate rocking limit state (b).

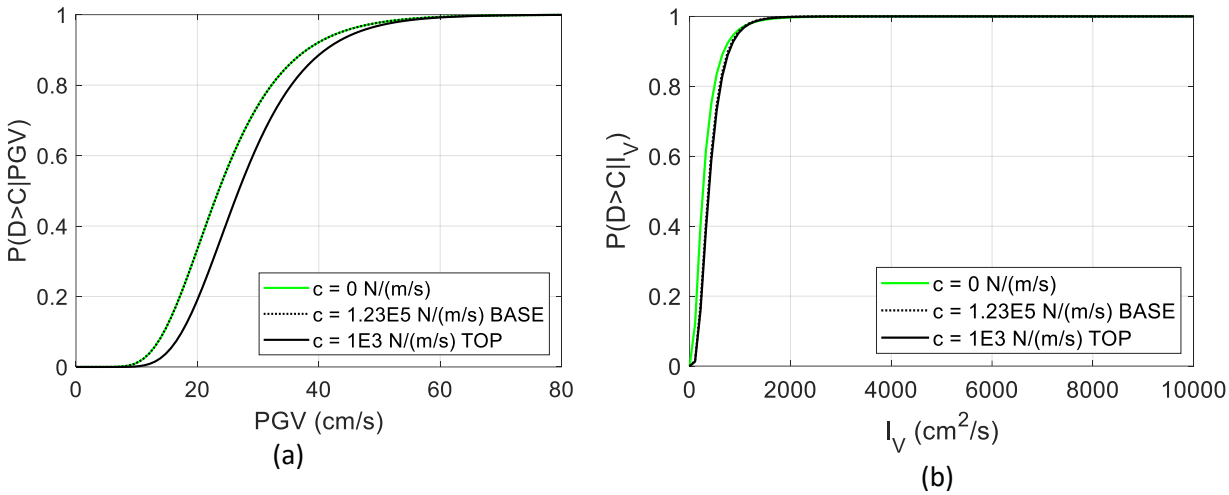

Figure 9: Fragility curves for stocky block IP, LS1, IMs: PGV (a); I_V (b).

As for the bivariate curves, the probability of exceedance of the three limit states is shown in Figure 10a comparing the response of the free-standing slender block to that of the block restrained by the top dissipator.

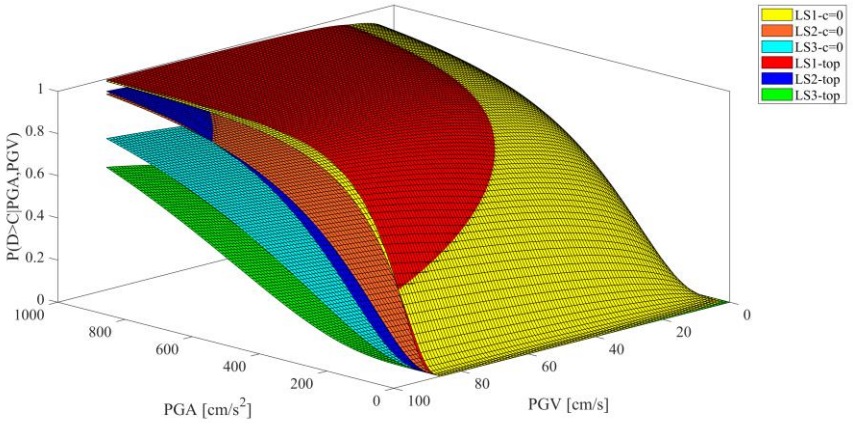

(a)

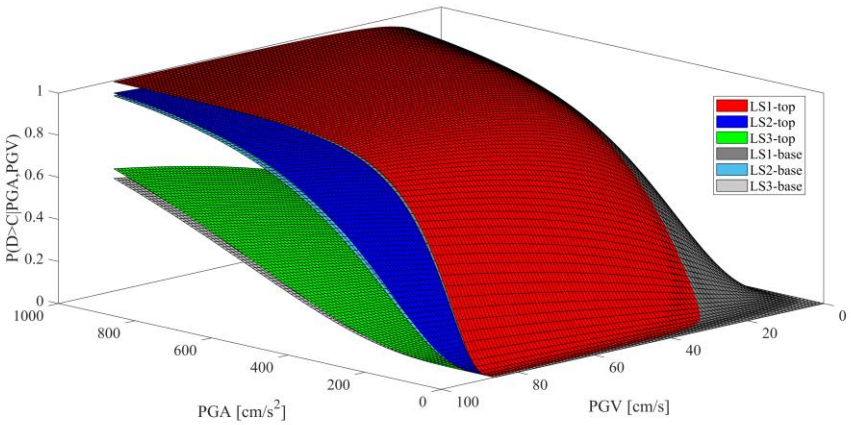

(b)

Figure 10: Bivariate fragility curves for slender block OOP, all limit states: comparison between undamped and damped configuration c_{top}=1 kN/(m/s) (a); comparison damped configuration c_{top}=1 kN/(m/s) and c_{base}=123 kN/(m/s) (b).

It is visible the improvement obtained in the case of earthquake-resistant device for low-medium intensity earthquakes. Actually, there is a superposition of the two surfaces corresponding to the limited rocking and, to a lesser extent, to the moderate rocking limit states, since for high values of PGA and PGV, the normalized rotations of the response with dashpot are similar to those of the undamped case. A re-centering device stabilizes the response as occurred in the deterministic analysis. Figure 10b shows the comparison between the two equivalent damped cases: a good agreement between the fragility curves is observed, with slight differences at the tails of the surfaces.

5 CONCLUSIONS

This paper presented an equivalence criterion for calculating the damping properties of dissipative devices located either at the base or at the top of rocking rigid blocks. These two configurations can be considered for non-structural elements such as precast panels in a perspective of low-damage or damage avoidance design. The proposed equivalence criterion was validated for a deterministic analysis applied on two blocks with different slenderness, rocking in-plane and out-of-plane. This criterion was also used in the stochastic analysis. In all the cases, rocking analyses showed very satisfactory agreement in terms of time-history response and in terms of fragility curves. As for the stochastic analysis, the optimal IMs were based on velocity, i.e., peak ground velocity PGV and energy density IV. Furthermore, the reduction of seismic vulnerability in the case of damped rocking was more visible considering limit states of moderate and near-collapse rocking. The paper also discussed the beneficial effects of dissipative and re-centering components on the rocking response of the blocks. The re-centering component further stabilized the rocking behavior, making it smoother and improving the agreement between the response for a dashpot installed at the base and that for a dashpot at the top of the rigid block.

ACKNOWLEDGEMENTS

This research was financed by Sapienza University of Rome, within the project “ANalytical Unified Modelling of A New earthquake-resistant device for the reduction of seismic vulnerability of masonry buildings (ANUMAN)” n. protocol RP1221814E212601 and by Regione Lazio (Progetto Fare Ricerca anno 2022).

REFERENCES

[1] S. Pampanin, Towards the “Ultimate Earthquake-Proof” Building: Development of an Integrated Low-Damage System, *Perspectives on European Earthquake Engineering and Seismology: Volume 2*, A. Ansal, Ed. Cham: Springer International Publishing, 2015, pp. 321–358. doi: 10.1007/978-3-319-16964-4_13.

[2] E. G. Dimitrakopoulos, M. J. Dejong, Seismic Overturning of Rocking Structures with External Viscous Dampers, *Computational Methods in Earthquake Engineering*, vol. 30, 2013.

[3] M. Froli, L. Giresini, and F. Laccone, Dynamics of a new seismic isolation device based on tribological smooth rocking (TROCKSISD), *Engineering Structures*, vol. 193, pp. 154–169, Aug. 2019, doi: 10.1016/j.engstruct.2019.05.014.

[4] L. Giresini, M. L. Puppio, F. Laccone, and M. Froli, Experimental and numerical investigation on a passive control system for the mitigation of vibrations on SDOF and MDOF Structures: mini Tribological ROCKing Seismic Isolation Device (mini-TROCKSISD), *Journal of Earthquake Engineering*, vol. 26, no. 14, pp. 7486–7504, Oct. 2022, doi: 10.1080/13632469.2021.1964646.
[5] N. Makris and M. F. Vassiliou, Dynamics of the Rocking Frame with Vertical Restrainers, *Journal of Structural Engineering*, vol. 141, no. 10, 2015.
[6] N. Makris and C. J. Black, Uplifting and Overturning of Equipment Anchored to a Base Foundation, *Earthquake Spectra*, vol. 18, no. 4, pp. 631–661, 2002, doi: 10.1193/1.1515730.
[7] O. AlShawa, L. Liberatore, D. Liberatore, F. Mollaioli, and L. Sorrentino, Seismic Demand on a Unreinforced Masonry Wall Restrained by Elasto-Plastic Tie-Rods Under Earthquake Sequences, *International Journal of Architectural Heritage*, vol. 13, no. 7, pp. 1124–1141, 2019, doi: 10.1080/15583058.2019.1645239.
[8] M. Aghagholizadeh and N. Makris, Earthquake response analysis of yielding structures coupled with vertically restrained rocking walls, *Earthq Eng Struct Dyn*, vol. 47, no. 15, pp. 2965–2984, Dec. 2018, doi: https://doi.org/10.1002/eqe.3116.
[9] O. AlShawa, D. Liberatore, and L. Sorrentino, Dynamic One-Sided Out-Of-Plane Behavior of Unreinforced-Masonry Wall Restrained by Elasto-Plastic Tie-Rods, *International Journal of Architectural Heritage*, vol. 13, no. 3, pp. 340–357, Apr. 2019, doi: 10.1080/15583058.2018.1563226.
[10] R. P. Kennedy and M. K. Ravindra, Seismic fragilities for nuclear power plant risk studies, *Nuclear Engineering and Design*, vol. 79, no. 1, pp. 47–68, 1984, doi: https://doi.org/10.1016/0029-5493(84)90188-2.
[11] S. W. Swan and R. Kassawara, The use of earthquake experiences data for estimates of the seismic fragility of standard industrial equipment, *ATC 29-1 Proc of Seminar on Seismic Design, Retrofit and Performance of Nonstructural Components, Applied Technology Council*, 1998, pp. 313–322.
[12] G. Cremen and J. W. Baker, Improving FEMA P-58 non-structural component fragility functions and loss predictions, *Bulletin of Earthquake Engineering*, vol. 17, no. 4, pp. 1941–1960, 2019, doi: 10.1007/s10518-018-00535-7.
[13] M. A. Jaimes, M. M. Chávez, F. Peña, and A. D. García-Soto, Out-of-plane mechanism in the seismic risk of masonry façades, *Bulletin of Earthquake Engineering*, vol. 19, no. 3, pp. 1509–1535, 2021, doi: 10.1007/s10518-020-01029-1.
[14] L. Sorrentino, O. AlShawa, and L. D. Decanini, The relevance of energy damping in unreinforced masonry rocking mechanisms. Experimental and analytic investigations, *Bulletin of Earthquake Engineering*, vol. 9, no. 5, pp. 1617–1642, 2011, doi: 10.1007/s10518-011-9291-1.
[15] G. W. Housner, The behavior of inverted pendulum structures during earthquakes, *Bulletin of the Seismological Society of America*, vol. 53, no. 2, pp. 403–417, 1963, doi: 10.1017/CBO9781107415324.004.
[16] E. G. Dimitrakopoulos and T. S. Paraskeva, Dimensionless fragility curves for rocking response to near-fault excitations, *Earthq Eng Struct Dyn*, vol. 44, no. 12, pp. 2015–2033, 2015, doi: 10.1002/eqe.2571.
[17] L. Giresini, Effect of dampers on the seismic performance of masonry walls assessed through fragility and demand hazard curves, *Engineering Structures*, vol. 261, p. 114295, Jun. 2022, doi: 10.1016/j.engstruct.2022.114295.
[18] L. Giresini, Design strategy for the rocking stability of horizontally restrained masonry walls, *COMPDYN 2017 6th ECCOMAS Thematic Conference on Computational Meth-*

ods in Structural Dynamics and Earthquake Engineering, Rhodes Island, Greece, 15–17 June 2017., 2017.
[19] L. Giresini, F. Taddei, F. Solarino, G. Mueller, and P. Croce, Influence of Stiffness and Damping Parameters of Passive Seismic Control Devices in One-Sided Rocking of Masonry Walls, *Journal of Structural Engineering*, vol. 148, no. 2, p. 04021257, Feb. 2022, doi: 10.1061/(asce)st.1943-541x.0003186.
[20] G. W. Housner, The behavior of inverted pendulum structures during earthquakes, *Bulletin of the Seismological Society of America*, vol. 53, no. 2, pp. 403–417, 1963, doi: 10.1017/CBO9781107415324.004.
[21] M. Aslam, W. G. Godden, and D. T. Scalise, Rocking and Overturning Response of Rigid Bodies to Earthquake Motions, *Lawrence Berkeley National Laboratory*, vol. Berkeley, p. 86 p., 1978.
[22] P. R. Lipscombe and S. Pellegrino, Free rocking of prismatic blocks, *Journal of Structural Engineering*, vol. 119, no. 7, pp. 1387–1410, 1993, doi: 10.1061/(ASCE)0733-9399(1993)119:7(1387).
[23] N. Makris and J. Zhang, Rocking Response and Overturning of Anchored Equipment under Seismic Excitations: Report 06 Sept. 1999.
[24] C. Casapulla, L. Giresini, L. U. Argiento, and A. Maione, Nonlinear Static and Dynamic Analysis of Rocking Masonry Corners Using Rigid Macro-Block Modeling, *International Journal of Structural Stability and Dynamics*, vol. 19, no. 11, p. 1950137, 2019, doi: 10.1142/S0219455419501372.
[25] L. Giresini, F. Solarino, O. Paganelli, D. V. Oliveira, and M. Froli, One-sided rocking analysis of corner mechanisms in masonry structures: influence of geometry, energy dissipation, boundary conditions, *Soil Dynamics and Earthquake Engineering*, vol. 123, pp. 357–370, 2019.
[26] M. Froli, L. Giresini, and F. Laccone, Dynamics of a new seismic isolation device based on tribological smooth rocking (TROCKSISD), *Eng Struct*, vol. 193, pp. 154–169, 2019.
[27] L. Giresini, F. Solarino, F. Taddei, and G. Mueller, Experimental estimation of energy dissipation in rocking masonry walls restrained by an innovative seismic dissipator (LICORD), *Bulletin of Earthquake Engineering*, vol. 19, no. 5, pp. 2265–2289, Mar. 2021, doi: 10.1007/s10518-021-01056-6.
[28] C. Casapulla, On the resonance conditions of rigid rocking blocks, *International Journal of Engineering and Technology*, vol. 7, no. 2, pp. 760–771, 2015.
[29] A. K. Chopra, *Dynamics of Structures*, 4th ed. Pearson, 2012.
[30] F. Solarino and L. Giresini, Fragility curves and seismic demand hazard analysis of rocking walls restrained with elasto-plastic ties, *Earthq Eng Struct Dyn*, vol. 50, no. 13, pp. 3602–3622, Oct. 2021, doi: 10.1002/eqe.3524.
[31] E. G. Dimitrakopoulos, N. Makris, and A. J. Kappos, Dimensional analysis of the earthquake-induced pounding between adjacent structures, *Earthq Eng Struct Dyn*, vol. 38, no. 7, pp. 867–886, 2009.
[32] L. Cabanas, B. Benito, and M. Herraiz, An approach to the measurement of the potential structural damage of earthquake ground motions, *Earthq Eng. Struct. Dyn.*, vol. 26, pp. 79–92, 1997.
[33] M. D. Trifunac and A. G. Brady, A study on the duration of strong earthquake ground motion, *Bulletin of the Seismological Society of America*, vol. 65, no. 3, pp. 581–626, 1975.
[34] E. M. Rathje, F. Faraj, S. Russell, and J. D. Bray, Empirical Relationships for Frequency Content Parameters of Earthquake Ground Motions, *Earthquake Spectra*, vol. 20, no. 1, pp. 119–144, 2004, doi: 10.1193/1.1643356.

[35] L. Giresini, C. Casapulla, R. Denysiuk, J. Matos, and M. Sassu, Fragility curves for free and restrained rocking masonry façades in one-sided motion, *Engineering Structures*, vol. 164, pp. 195–213, 2018, doi: https://doi.org/10.1016/j.engstruct.2018.03.003.

[36] L. Luzi, R. Puglia, E. Russo, and O. WG5, *Engineering Strong Motion Database, version 1.0*, Istituto Nazionale di Geofisica e Vulcanologia, Observatories & Research Facilities for European Seismology. 2016.

[37] L. Sorrentino, D. D'Ayala, G. de Felice, M. C. Griffith, S. Lagomarsino, and G. Magenes, Review of Out-of-Plane Seismic Assessment Techniques Applied To Existing Masonry Buildings, *International Journal of Architectural Heritage*, vol. 11, no. 1, pp. 2–21, 2017, doi: 10.1080/15583058.2016.1237586.